INCLUSIONS IN TRANSPARENT GEM RHODONITE FROM BROKEN HILL, NEW SOUTH WALES, AUSTRALIA

Paul W. Millsteed, Terrence P. Mernagh, Vincent Otieno-Alego, and Dudley C. Creagh

Solid, vapor, and fluid inclusions in transparent gem rhodonite crystals from Broken Hill, New South Wales, Australia, have been identified for the first time using Raman spectroscopy and gemological/petrographic techniques. Among the solid inclusions are sphalerite, galena, quartz, and fluorite. The rhodonite also contained hollow needle-like tubes and negative rhodonite crystals. Three-phase inclusions were found to contain a saline liquid, a gaseous mixture of nitrogen (N_2) and methane (CH_4), and ilmenite crystals.

Gem rhodonite crystals have been recorded from Broken Hill, New South Wales, Australia, for at least 100 years. Most of these crystals have been recovered from the North mine and Zinc Corp./NBHC mines; however, they are widely distributed throughout the deposit. A number of beautiful transparent crystals, less than 1 cm thick, have been recorded (Birch, 1999; see, e.g., figure 1), with some rare specimens as large as several centimeters across. The authors know of at least six crystals that have been successfully faceted, producing stones that range from 0.15 to 10.91 ct, and these display a rich pink to brownish red color similar to that seen in pink-to-red spinel. The 10.91 ct stone (figure 2), the largest faceted rhodonite ever recorded from Broken Hill, is currently on display at Toronto's Royal Ontario Museum. No rhodonite cabochons from this locality have been documented. Because so little is known about this gem material, this article characterizes a variety of inclusions found in gem rhodonite from the North mine at Broken Hill.

BACKGROUND

Gem-quality rhodonite ($[Mn,Fe,Ca]SiO_3$) is known from the primary silver-lead-zinc sulfide orebodies centered at Broken Hill, arguably the most famous mining town in Australia (figure 3) and one of the richest sources of gem rhodonite crystals in the world.

Location. Broken Hill lies on the inland edge of the Western Plains of New South Wales at the foot of the Barrier Ranges, on the edge of the Sundown Hills, 1,100 km from Sydney and 43 km from the border with South Australia (Solomon, 1988). The Broken Hill deposit, renowned as one of the most outstanding mineral deposits in the world, is hosted in what geologists have defined as the Broken Hill block. Some 2,000 separate mineral deposits are distributed throughout the block, over an area of 4,000 km^2 (Barnes, 1986).

Regional Geology and Occurrence of Rhodonite. Up to nine separate, but closely related, lenses and lodes are hosted in rocks of the Willyama Supergroup at Broken Hill (Stevens et al., 1983). Differences in the orebodies are reflected in the relative proportions of lead and zinc, as represented by the minerals galena and sphalerite, respectively (Johnson and Klinger, 1975; Plimer, 1979, 1984). In addition to these two minerals, rhodonite from Broken Hill may be associated with spessartine, calcite, hedenbergite, bustamite, fluorapatite, fluorite, quartz, and pyroxmangite (Birch, 1999).

See end of article for About the Authors and Acknowledgments.
GEMS & GEMOLOGY, Vol. 41, No. 3, pp. 246–254.

Figure 1. The Broken Hill mines in New South Wales, Australia, have produced attractive gem-quality rhodonite crystals, such as this 2.9-cm-long prism. Photo by Wendell Wilson, courtesy of The Mineralogical Record.

Most of the orebodies at Broken Hill have a granular texture in both non-ore (gangue) and sulfide portions. Specimens of ore collected from 3 Lens, one of the two known lead lodes at North mine, typically display this texture (figure 4). Local geologists refer to the lead lodes as having layering in the ore, known to enclose pods and "boudins" (sausage-shaped segments) of low-grade rhodonite, bustamite or manganhedenbergite, other gangue minerals, and sulfides. Overall, masses of rhodonite and bustamite have exceeded 20 m across (Maiden, 1975).

History of Mining at Broken Hill. The Broken Hill orebody was pegged in September 1883 and later subdivided into seven mining leases called blocks (which are distinct from the Broken Hill block discussed above). Block 17, then known as the "Cosmopolitan," was established in December 1883 and acquired by the North Broken Hill Silver Mining Co. in 1885 (figure 5). Although some secondary silver and lead ore was mined in 1888, this was rapidly exhausted, and in 1897 the North Broken Hill Silver Mining Co. began mining the primary sulfide ore.

North Broken Hill Ltd. acquired Block 17 in 1912 and established itself as a major employer in the city of Broken Hill (Koenig, 1983). During peak production, between 1970 and 1975, some 800–900 workers were employed by North Broken Hill Ltd. at this operation.

The North mine leases comprise mainly those parts of the deposit that geologists have referred to as the lead lodes 3 Lens and 2 Lens. In the 1970s, miners working the stopes of the 25, 26, and 27 levels of No. 3 shaft, some 350 m from the surface, made a concerted effort to ensure the preservation of a significant quantity of rhodonite crystals by skillfully separating them from the sulfide orebody. These intense pinkish to brownish red translucent-to-opaque tabular crystals, reaching up to 10 cm

Figure 2. This 10.91 ct modified emerald step cut is believed to be the largest faceted rhodonite from the Broken Hill mines. The stone was cut by Maria Atkinson and is currently on display at the Royal Ontario Museum, Toronto. Photo by David Atkinson.

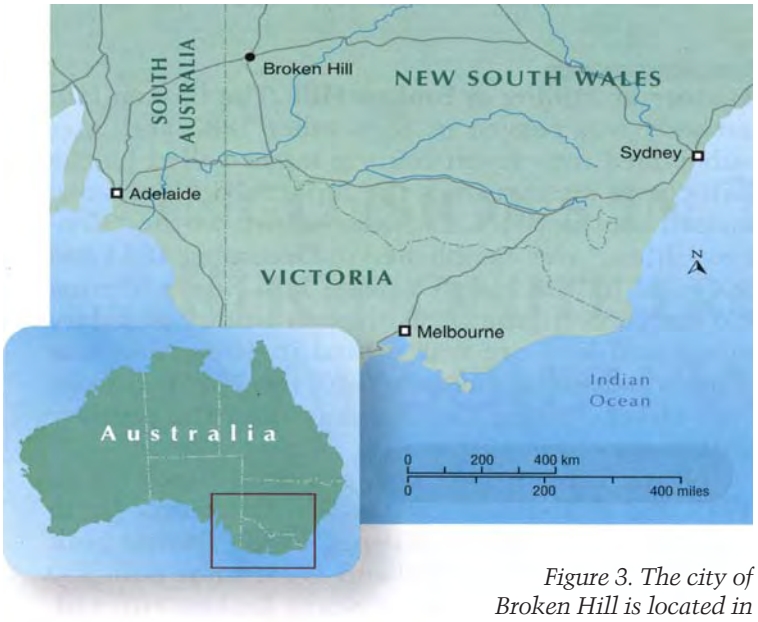

Figure 3. The city of Broken Hill is located in western New South Wales, Australia. The North mine is located in the northern part of the mining field.

across, were occasionally associated with random clusters and pockets of beautiful transparent crystals about 1 cm wide. These specimens soon became highly prized by the wider mineralogical community in Broken Hill and beyond.

Many Australian museums and private collectors have preserved some outstanding specimens of this transparent rhodonite from the Broken Hill orebody, both in matrix (e.g., figure 6) and as individual crystals (again, see figure 1). North Broken Hill Ltd. closed its operations in 1993, but development plans for a smaller mining operation by the current lease-holder, Perilya Pty Ltd., are now under way.

Reported Properties of Broken Hill Rhodonite. The typical composition of rhodonite from Broken Hill is 50–70 mol.% $MnSiO_3$, 18–20 mol.% $CaSiO_3$, and 10–20 mol.% $FeSiO_3$; traces of Zn and Mg may also be present (Albrecht and Peters, 1980). Absorption bands at 523–536 nm (19100–18650 cm^{-1}), caused by Fe^{2+} and Mn^{2+}, are typical for transparent gem rhodonite from the North mine (Bank et al., 1974). Refractive indices for similar specimens were recorded by Diehl and Berdesinski (1970) as n_α = 1.725, n_β = 1.729, and n_γ = 1.737. Generally speaking, rhodonite has a density in the range 3.55–3.76 g/cm^3 (Gaines et al., 1997). Bank et al. (1974) reported a value of 3.74 g/cm^3 for one transparent specimen from Broken Hill.

A recent investigation into the faceting of transparent rhodonite from Broken Hill revealed a notable suite of solid and fluid inclusions, which we subsequently studied by Raman spectroscopy and petrographic techniques, as reported here.

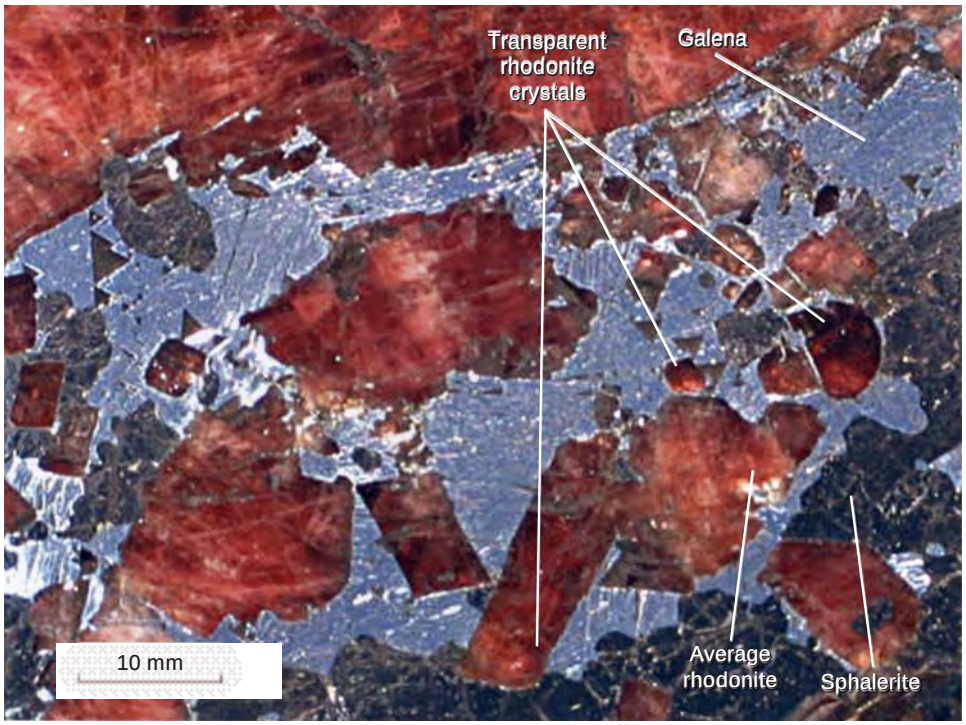

Figure 4. This polished ore sample from the 25/26 level of the North mine (specimen 1) contains crystals of galena (3–8 mm), sphalerite (3–10 mm), and subhedral to euhedral rhodonite (2–70 mm). Note the several transparent rhodonite crystals. Photomicrograph by Paul Millsteed.

Figure 5. The North Broken Hill Silver Mining Co. acquired Block 17 at Broken Hill, which would later become known as the North mine, in 1885. This photo of the mining operation was taken in 1888 (from Koenig, 1983).

MATERIALS AND METHODS

Eight transparent rhodonite crystals (5–25 mm long), recovered from 3 Lens, 25/26 level, of the North mine were prepared and examined. Six of the crystals (specimens 4–9) were sliced, resulting in 12 sections that were polished on both sides for optimal inclusion identification. The thickness of the sections ranged from 100 μm to 2 mm, and most contained subsurface solid or fluid inclusions ranging from <1 μm to 100 μm in diameter. One crystal, specimen 3, was retained intact for the duration of the experimental work. We determined gemological properties (including visible absorption spectra) using standard gemological instruments on specimen 2, a faceted stone (figure 7). (Specimen 1 was the ore sample shown in figure 4.)

Figure 6. This specimen of rhodonite crystals embedded in calcite (3 × 2.5 × 2 cm, from level 17 of the Zinc Corp. mine) is part of the Albert Chapman Collection at the Australian Museum, Sydney. Photo by Carl Bento, Australian Museum (No. D49967).

Figure 7. Gemological properties were taken on this 0.86 ct faceted rhodonite (5.4 × 5.4 × 3.9 mm; specimen 2) from the North mine at Broken Hill, which was cut by Ralph Westen. Photo by Paul Millsteed.

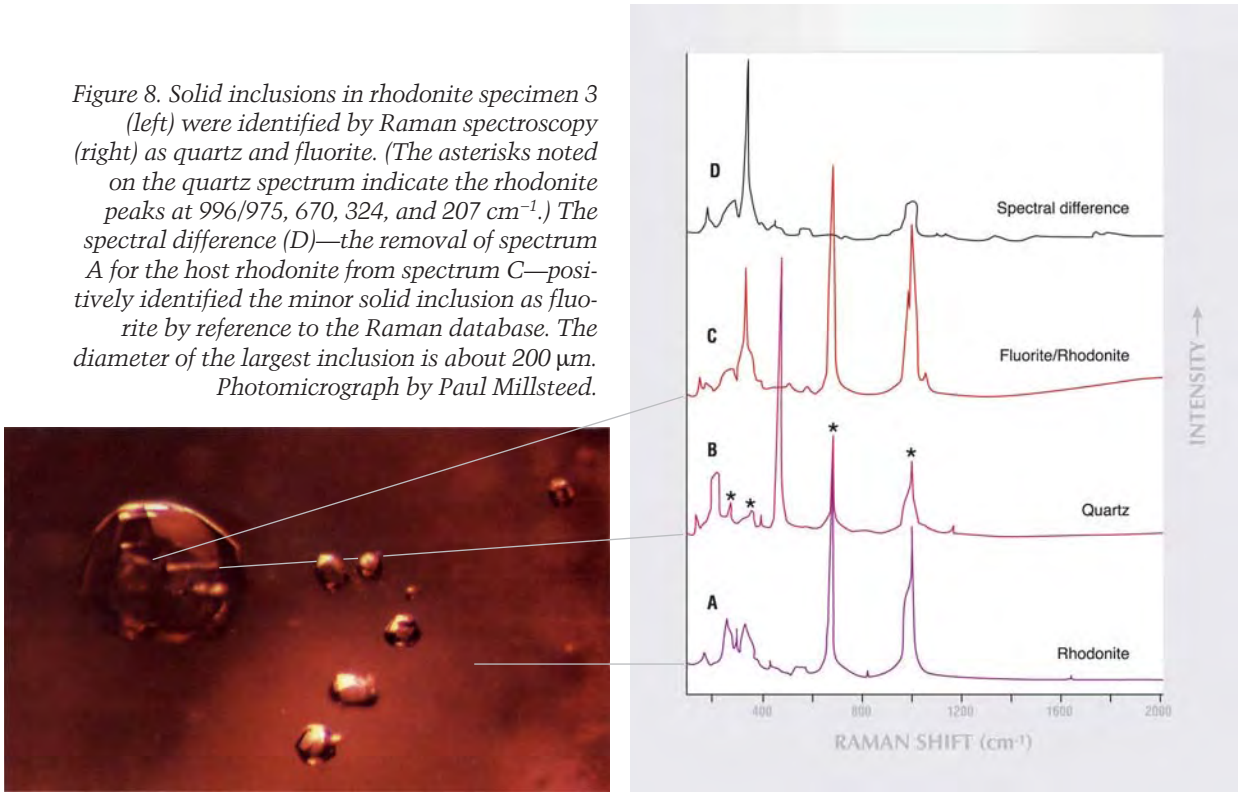

Figure 8. Solid inclusions in rhodonite specimen 3 (left) were identified by Raman spectroscopy (right) as quartz and fluorite. (The asterisks noted on the quartz spectrum indicate the rhodonite peaks at 996/975, 670, 324, and 207 cm^{-1}.) The spectral difference (D)—the removal of spectrum A for the host rhodonite from spectrum C—positively identified the minor solid inclusion as fluorite by reference to the Raman database. The diameter of the largest inclusion is about 200 μm. Photomicrograph by Paul Millsteed.

Microscopic observations of specimens 3–9 were initially performed using a Leica DMR polarizing microscope. The types of inclusions, their sizes and shapes, and the number of phases they contained were noted for these specimens, as well as for a 15 × 20 × 35 mm rhodonite crystal in a matrix of galena (specimen 10, the eighth transparent crystal).

Raman spectra were recorded for solid inclusions in specimen 3 using a Renishaw Raman microspectrometer with a 632.8 nm He-Ne laser as the excitation source. The instrument was used in confocal mode for maximum spatial resolution. With this setting, individual solid inclusions initially pinpointed using transmitted light were targeted by focusing the laser beam via the 50× microscope objective.

Raman spectra for the vapor phase of three-phase inclusions were also recorded *in situ* for one of the sections cut from specimen 4 using a Dilor SuperLabram microspectrometer. These inclusions were analyzed with a higher-energy 514.5 nm laser excitation. A 100× microscope objective was used to increase the laser intensity at the focal point within the inclusions. The spectra of the vapor phase were recorded from 3800 to 1000 cm^{-1} using a single 20-second integration time per spectrum. The detection limits for specific gases are dependent on the

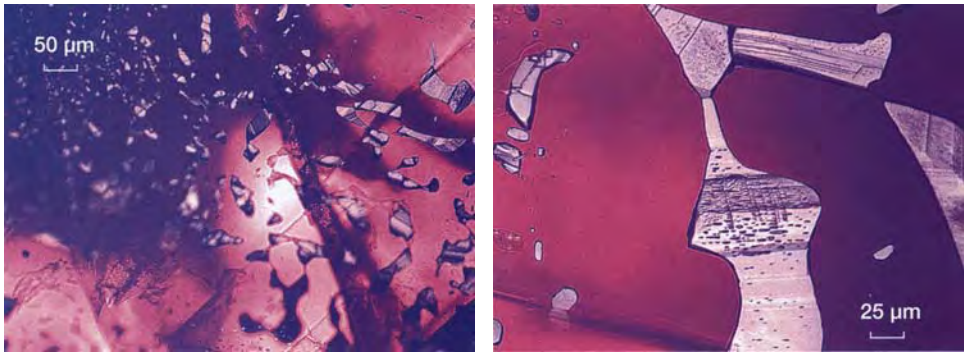

Figure 9. Many of the samples contained galena inclusions, as seen here along fractures in specimen 6. A closer view (right) shows contact-twin lamellae evident as diagonal striations along cleavages, together with a surficial fluid. Photomicrographs by Paul Millsteed; transmitted light.

Figure 10. Many samples also contained sub-angular elongate sphalerite inclusions, such as those shown here in specimen 7. Photomicrograph by Paul Millsteed.

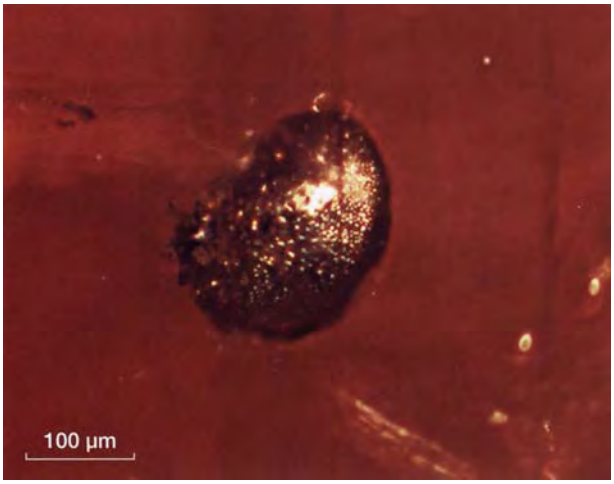

Figure 11. A number of rounded pyrrhotite grains were seen in specimen 10, but not in any of the other samples examined. Pyrrhotite has been found throughout the Broken Hill ore deposit. Photomicrograph by Paul Millsteed; reflected light.

instrumental sensitivity, the partial pressure of each gas, and the optical quality of each fluid inclusion. Raman detection limits (Wopenka and Pasteris, 1987) are estimated to be around 0.1 mol.% for CO_2, O_2, and N_2, and about 0.03 mol.% for H_2S and CH_4. Errors in the calculated gas ratios are generally less than 1 mol.%.

RESULTS

Gemological Properties. The refractive indices determined from specimen 2 were $n_\alpha = 1.732$ and $n_\gamma = 1.745$. Pleochroism was generally weak, showing colors of yellowish red, pinkish red, and pale yellowish red. The optic axis angle (2V) yielded a biaxial positive optic sign. The dominant morphological forms were (001), (1$\bar{1}$0), and (110). Specific gravity determinations yielded a value of 3.65.

The visible absorption spectra revealed lines at 408 and 412 nm and a diffuse weak band at 455 nm. A strong narrow absorption line at 503 nm and a broad band at 548 nm were also recorded. The sample fluoresced a dull dark red to both long- and short-wave UV radiation.

Raman and Petrographic Analyses of Inclusions. Figure 8 illustrates a large solid inclusion (about 200 µm in diameter) that contained two solid phases. After subtraction of the rhodonite peaks at 996 and 975 cm^{-1}, one of these phases was identified as quartz and the other as fluorite. A suite of solid inclusions identified using petrological techniques included elongate or rounded twinned galena (figure 9), with contact-twin lamellae evident as diagonal striations along cleavages together with residual fluid, as well as sub-angular elongate sphalerite (figure 10) and rounded pyrrhotite crystals (figure 11).

Also seen were several generations of negative crystals that were commonly aligned in preferred crystallographic orientations (figure 12); euhedral negative rhodonite crystals that formed in areas containing sphalerite (figure 13); and thin tubes that appeared to be hollow, from which no Raman signals could be recorded.

A number of specimens had three-phase inclusions, such as the suite shown in figure 14. These inclusions typically contained CH_4 and N_2 in the vapor phase (figure 15), a liquid of moderate to high salinity (based on the maximum around 3450 cm^{-1} and the low intensity of the peak at 3300 cm^{-1}), and a solid identified as ilmenite (figure 16).

Figure 14A shows a suite of euhedral negative crystals. A particularly large negative crystal in this suite contained a vapor bubble (~15 vol.%) and an opaque solid (~5 vol.%). Raman analysis of that vapor phase revealed 49 mol.% CH_4 and 51 mol.% N_2; the vapor phase of a similar inclusion in figure 14B contained 53 mol.% CH_4 and 47 mol.% N_2. The needle-like inclusions with negative crystal shapes (which were commonly aligned along preferred crystallographic orientations) had the same chemical composition but different phase ratios. For example, the needle-like inclusion in figure 14D contained 30 vol.% vapor ($CH_4 \pm N_2$), 50 vol.% saline liquid, and 20 vol.% ilmenite. We

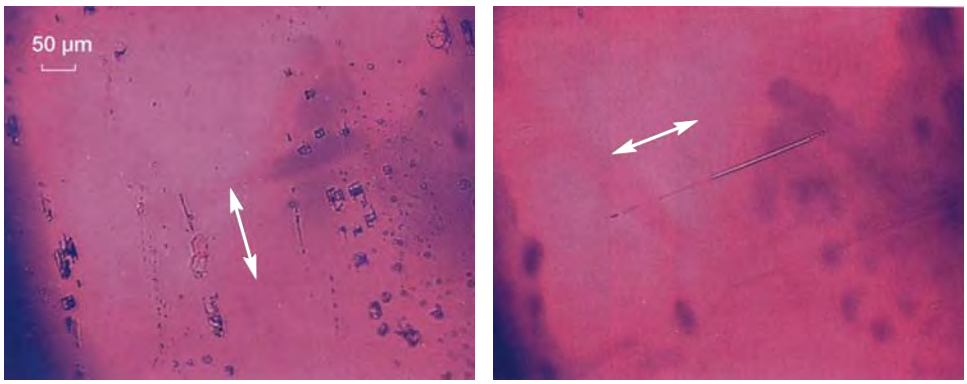

Figure 12. Also seen (here, in specimen 5) were several generations of hollow negative crystals aligned along a preferred crystallographic orientation, as shown by the white arrows. Photomicrographs by Paul Millsteed.

believe this is due to leakage of fluid from the inclusions along the healed fractures, such as those that are evident at each end of the inclusion in figure 14D.

Several additional photomicrographs and Raman spectra of the inclusions identified in this study are available in the *Gems & Gemology* Data Depository at www.gia.edu/gemsandgemology.

DISCUSSION

The gemological properties obtained in this study were consistent with those for rhodonite in the literature, although the R.I. values were higher than those given by Diehl and Berdesinski (1970) and Bank et al. (1973a). While pyroxmangite is recognized from Broken Hill, all the specimens reported here have typical rhodonite compositions and properties.

Figure 13. Situated among the inclusions of sphalerite in specimen 8 was a euhedral negative crystal of rhodonite. Photomicrograph by Paul Millsteed.

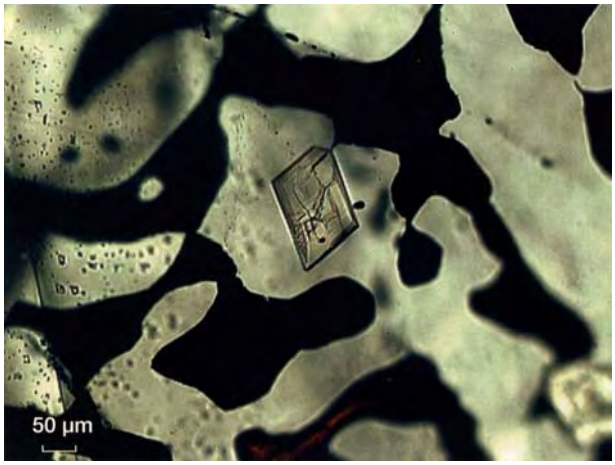

This study identified a diverse group of inclusions in transparent gem rhodonite from the North mine at Broken Hill. Previous studies of gem rhodonite from this locality (Diehl and Berdesinski, 1970; Bank et al., 1973a,b and 1974; Gaines et al., 1997) have not mentioned the presence of inclusions.

The basic gemological properties of Brazilian rhodonite appear to be comparable to those of rhodonite from Broken Hill. Faceted rhodonite from Minas Gerais, Brazil, was recently found to contain curved needles, "fingerprints," and two-phase inclusions (Quinn, 2004), but no solid inclusions were identified.

We believe that the inclusions in the Broken Hill rhodonite originate from metamorphic reactions that may have produced fluids through processes of dehydration and decarbonation (Stevenson and Martin, 1986). It is probable that partial melting and plastic flow of the sulfides occurred in the Broken Hill ore deposit during peak metamorphism (Maiden, 1976), which may be evidence of high-temperature fluid activity (Plimer, 1979).

Experimental studies of the PbS-FeS-ZnS-Ag_2S system by Mavrogenes et al. (2001) showed that eutectic melting of sulfide occurs between 772° and 830°C. In the Broken Hill region, metamorphism was accompanied by folding, which changed the original structure, texture, and mineralogical content of the Broken Hill ore deposit. While the sulfide minerals galena and sphalerite have an average grain size of 3–4 mm (Birch, 1999), microscopic pyrrhotite and other sulfide inclusions have also been trapped within the silicate mineralogy, including gem rhodonite. The presence of pyrrhotite in rhodonite supports the eutectic peak metamorphic conditions discussed.

The three-phase (saline liquid, CH_4-N_2 vapor, and ilmenite crystal) inclusions are considered

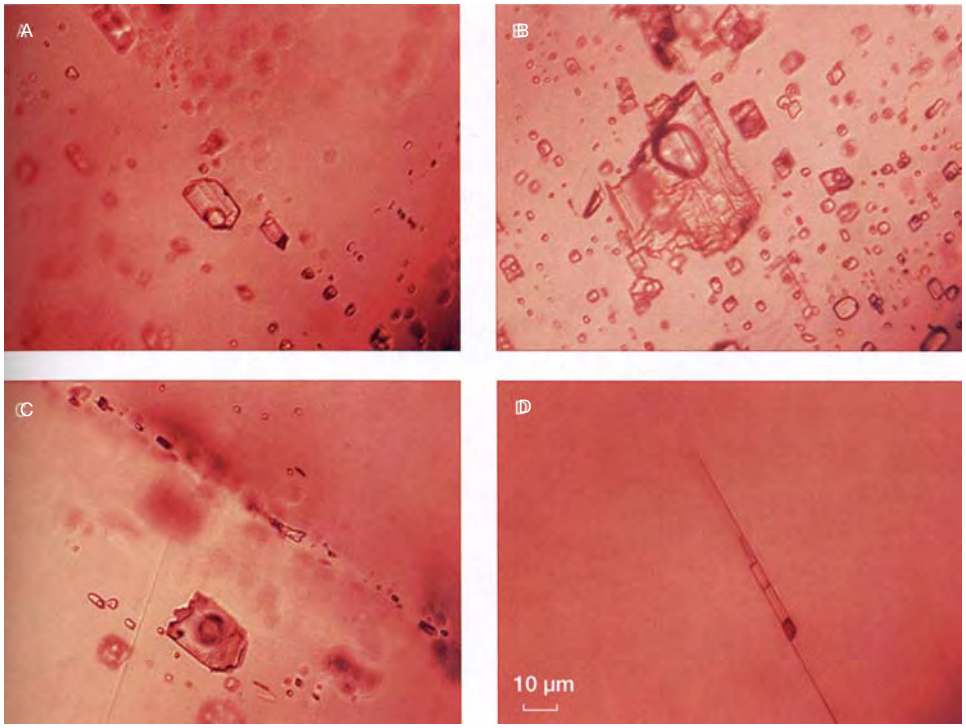

Figure 14. Specimen 4 contained numerous euhedral negative crystals with three phases: an ilmenite crystal, a saline liquid, and a CH_4-N_2 vapor. Photomicrographs by Paul Millsteed.

pseudosecondary. The binary mixture of N_2 and CH_4 in the vapor phase is in good agreement with previous studies of gases trapped in fluid inclusions from the gneissic host rocks and quartz veins of the Broken Hill ore deposit (Wilkins and Dubessy, 1984). The presence of inclusions of quartz, sub-angular elongate galena and sphalerite, and euhedral negative crystals of rhodonite with sphalerite may be characteristic of Broken Hill gem rhodonite. In addition, analysis of the fluid inclusions in gem rhodonite may indicate whether or not they originated from the Broken Hill orebody. Further research on inclusions in rhodonites from this and other localities is needed to make a definitive determination in this regard.

Figure 15. Raman spectroscopy of the vapor phase of the three-phase fluid inclusion in crystal specimen 4 confirmed the presence of N_2 and CH_4. CO_2, O_2, and H_2S were below the detection limits.

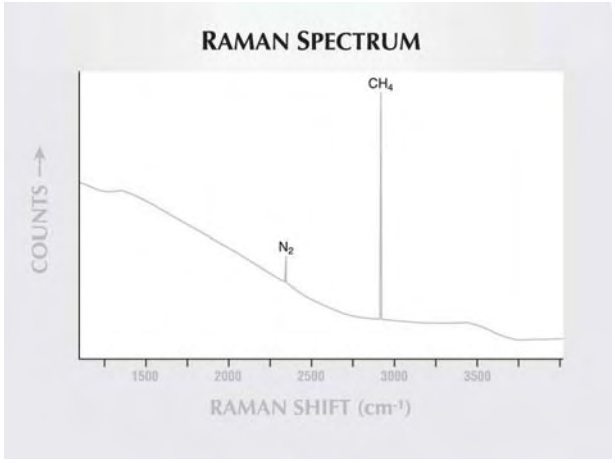

Figure 16. Raman spectroscopy also confirmed the presence of ilmenite crystals in a fluid inclusion in specimen 4, as illustrated in figure 14A. (The host rhodonite spectrum has been subtracted out, creating some "negative" peaks.)

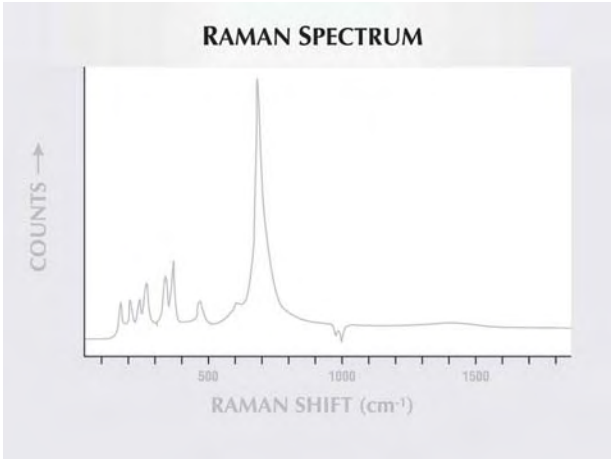

CONCLUSIONS

Sphalerite, galena, quartz, fluorite, and rare grains of pyrrhotite have been identified as solid inclusions in gem rhodonite from the Broken Hill area in New South Wales, Australia. Also identified for the first time in this material is a suite of three-phase (fluid, vapor, and solid) inclusions. These inclusions have trapped the products of dehydration, decarbonization, and partial melting during metamorphism at Broken Hill, forming (in partially healed fractures) after the rhodonite crystallized. The rhodonite crystals also contained hollow needle-like tubes, as no solids, liquids, or gases were detected in these features by Raman analysis. The solid and three-phase inclusions may serve as clues to the evolutionary metamorphic processes and help identify gem rhodonite as being from the Broken Hill deposit.

ABOUT THE AUTHORS

Mr. Millsteed (paulmillsteed@hotmail.com) is a visiting researcher, and Dr. Mernagh is a research scientist, with Geoscience Australia, Canberra, Australian Capital Territory. Dr. Otieno-Alego is a former research officer with the Corrosion and Spectroscopy Laboratory at the University of Canberra and is currently employed by the Australian Federal Police, Canberra. Dr. Creagh is director of the Corrosion and Spectroscopy Laboratory at the University of Canberra.

ACKNOWLEDGMENTS: The authors thank Arthur Main, lecturer in Gemmology with the Gemmological Association of Australia, Canberra, for his help with the manuscript. Dr. Mernagh publishes with the permission of the CEO of Geoscience Australia.

REFERENCES

Albrecht J., Peters T. (1980) The miscibility gap between rhodonite and bustamite along the join $MnSiO_3$ – $Ca_{0.60}Mn_{0.40}SiO_3$. *Contributions to Mineralogy and Petrology*, Vol. 74, pp. 261–269.

Bank H., Berdesinki W., Diehl R. (1973a) Durchsichtiger Rhodonit aus Broken Hill/Australien. *Zeitschrift der Deutschen Gemmologischen Gesellschaft*, Vol. 22, No. 3, pp. 101–103.

Bank H., Berdesinki W., Diehl R. (1973b) Durchsichtiger rötlicher Pyroxmangit aus Broken Hill/Australien und die Möglichkeiten seiner Unterscheidung von Rhodonit. *Zeitschrift der Deutschen Gemmologischen Gesellschaft*, Vol. 22, No. 3, pp. 104–110.

Bank H., Berdesinki W., Ottermann J., Schmetzer K. (1974) Transparent red iron rich rhodonite from Australia. *Zeitschrift der Deutschen Gemmologischen Gesellschaft*, Vol. 23, No. 3, pp. 180–188.

Barnes R.G. (1986) A summary record of mineral deposits in the Broken Hill block, excluding the southeastern portion. *Records of the Geological Survey of New South Wales*, Vol. 22, No. 2, pp. 1–367.

Birch W.D. (1999) *The Minerals of Broken Hill*. Broken Hill City Council and Museum, Victoria, New South Wales.

Diehl R., Berdesinski W. (1970) Twinning in pyroxmangite from the North mine in Broken Hill, New South Wales, Australia. *Neues Jahrbuch für Mineralogie Monatshefte*, Vol. 1970, No. 8, pp. 348–362.

Gaines R.V., Skinner H.C.W., Foord E.E., Mason B., Rosenzweig A., King V.T. (1997) *The System of Mineralogy of James Dwight Dana and Edward Salisbury Dana*, 8th ed. John Wiley & Sons, New York, pp. 1326–1328.

Johnson I.R., Klingner G.D. (1975) The Broken Hill ore deposit and its environment. In C.L. Knight, Ed., *The Economic Geology of Australia and Papua New Guinea*, Australasian Institute of Mining and Metallurgy, Melbourne, pp. 476–491.

Koenig K. (1983) *Broken Hill: 100 Years of Mining*. New South Wales Department of Mineral Resources, Sydney.

Maiden K.J. (1975) High grade metamorphic structures in the Broken Hill orebody. *Australian Institute of Mining and Metallurgy Proceedings*, Vol. 254, pp. 19–27.

Maiden K.J. (1976) Piercement structures formed by metamorphic mobilisation in the Broken Hill orebody. *Australasian Institute of Mining and Metallurgy Proceedings*, Vol. 257, pp. 1–8.

Mavrogenes J.A., MacIntosh I.W., Ellis D.J. (2001) Partial melting of the Broken Hill galena-sphalerite ore. Experimental studies in the system PbS-FeS-ZnS-(Ag_2S). *Economic Geology*, Vol. 96, No. 1, pp. 205–210.

Plimer I.R. (1979) Sulphide rock zonation and hydrothermal alteration at Broken Hill, Australia. *Transactions of the Institution of Mining and Metallurgy (London) B: Applied Earth Science*, Vol. 88, pp. B161–B187.

Plimer I.R. (1984) The mineralogical history of the Broken Hill lode, N.S.W. *Australian Journal of Earth Sciences*, Vol. 31, pp. 379–402.

Quinn E.P. (2004) Gem News International: Rhodonite of facet and cabochon quality from Brazil. *Gems & Gemology*, Vol. 40, No. 3, pp. 260–261.

Solomon R.J. (1988) *The Richest Lode, Broken Hill 1883–1988*. Hale and Iremonger, Sydney.

Stevens B.P.J., Willis I.L., Brown R.E., Stroud W.J. (1983) *The Early Proterozoic Willyama Supergroup: Definitions of Stratigraphic Units from the Broken Hill Block, New South Wales*. Geological Survey of New South Wales, Record 21, Maitland, pp. 407–442.

Stevenson R.K., Martin R.F. (1986) Implications of the presence of amazonite in the Broken Hill and Geco metamorphosed sulphide deposits. *Canadian Mineralogist*, Vol. 24, pp. 729–745.

Wilkins R., Dubessy J. (1984) Relative chronology of retrograde metamorphic fluids in the host rocks of the stratiform Broken Hill orebody (New South Wales, Australia). *Comptes Rendus de l'Académie des Sciences*, Vol. 299, Series II, No. 15, pp. 1045–1050.

Wopenka B., Pasteris J.D. (1987) Raman intensities and detection limits of geochemically relevant gas mixtures for a laser Raman microprobe. *Analytical Chemistry*, Vol. 59, No. 17, pp. 2165–2170.